Research Article

Link Gain Matrix Estimation in Distributed Large-Scale Wireless Networks

Jing Lei, Larry Greenstein, and Roy Yates

WINLAB, Department of ECE, Rutgers University, North Brunswick, NJ 08902, USA

Correspondence should be addressed to Jing Lei, michelle.j.lei@gmail.com

In planning and using large-scale distributed wireless networks, knowledge of the link gain matrix can be highly valuable. If the number N of radio nodes is large, measuring $N(N - 1)/2$ node-to-node link gains can be prohibitive. This motivates us to devise a methodology that measures a fraction of the links and accurately estimates the rest. Our method partitions the set of transmit-receive links into mutually exclusive categories, based on the number of obstructions or walls on the path; then it derives a separate link gain model for each category. The model is derived using gain measurements on only a small fraction of the links, selected on the basis of a maximum entropy. To evaluate the new method, we use ray-tracing to compute the "true" path gains for all links in the network. We use knowledge of a subset of those gains to derive the models and then use those models to predict the remaining path gains. We do this for three different environments of distributed nodes, including an office building with many obstructing walls. We find in all cases that the partitioning method yields acceptably low path gain estimation errors with a significantly reduced number of measurements.

1. Introduction

The powerful technology and market trends towards portable computing and communications imply an increasingly important role for wireless access in the next-generation Internet. Moreover, distributed and pervasive computing applications are proliferating and expected to drive large-scale deployments of embedded computing devices interconnected via wireless links. Large-scale distributed wireless networks arise in a variety of forms. Examples include sensor networks, wherein data processing is distributed among the nodes [1]; ad hoc mesh networks, wherein nodes act as relays for each other [2]; and the laboratory testbeds used to evaluate sensor and mesh network protocols [3]. In all these cases, the operation for the network can benefit from knowing the *link gain matrix*, which describes the transmitter-receiver power ratio among all the nodes in the network taken pairwise.

A particular application of the gain matrix in testbeds is described in [4, 5]. Motivated by the goal to advance the technology innovation in the wireless networking field, the Open Access Research Testbed for Next-Generation Wireless Networks (ORBIT) was built at Rutgers University's WINLAB facility [4, 5], which focuses on the creation of a large-scale wireless network testbed and aims to facilitate a broad range of experimental research on novel protocols and application concepts. The proposed ORBIT system employs a two-tier laboratory emulator/field trial network to achieve reproducibility of experimentation, and supports evaluation of protocols and applications in real-world settings illustrated in Figure 1(a). As shown by Figure 1(b), the laboratory-based wireless network emulator is constructed with a large two-dimensional array of 802.11x radio nodes (400 nodes), which are uniformly spaced on a square grid of 20 meters by 20 meters and can be dynamically interconnected into specified topologies for reproducible wireless channel models. The number of pairwise link gains in this case is about 80,000. Due to obstructing pillars as well as *multipath* from reflecting walls, floor, and ceiling, the link gains depart significantly from a simple free-space pathloss description. Unfortunately, conventional stochastic pathloss models (e.g., [6]) cannot be applied to laboratory testbed, and the alternative of making measurements over all node pairs can be impractical. Therefore, it is desirable to estimate
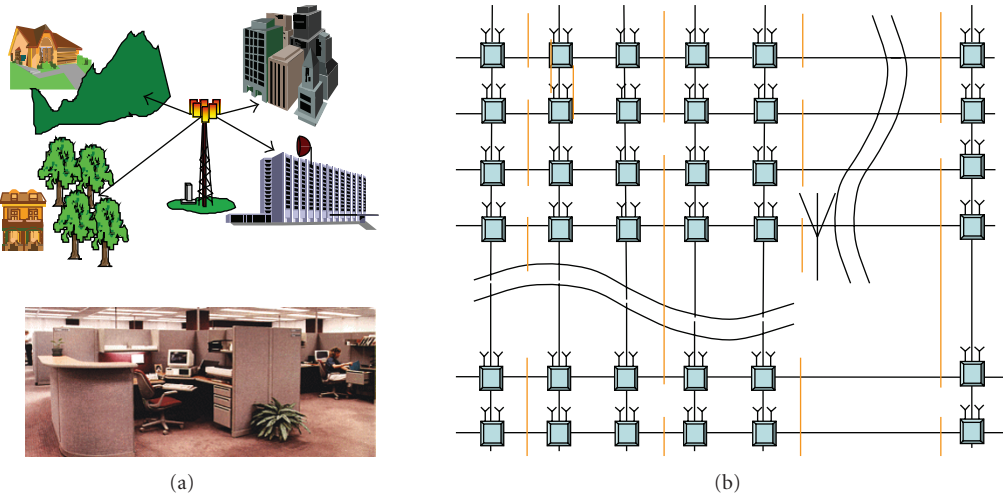
FIGURE 1: Mapping of real world environments onto the ORBIT indoor testbed. (a) Real world outdoor/indoor environment (b) 400-node ORBIT indoor testbed.

all the path gains, if possible, using only a small fraction of the full number of measurements.

In [7], we considered the use of spatial interpolation for pathloss estimation. In this approach, a subset of link gains is measured, and then we invoke the assumption of smooth spatial variations to infer all other path gains via interpolation. For the 400-node ORBIT testbed, we found that the use of spatial interpolation methods permitted reasonably accurate estimates to be obtained using only a few thousand measurements instead of 80,000. However, we report here on an alternative approach that provides even better accuracies with even fewer measurements. The key to this new approach, and what makes it novel, is that the set of all node-to-node paths is partitioned into 3 or more categories, and a separate stochastic model is derived for each. By using a suitable means of categorization, we find that each model of pathloss versus log-distance fits a simple mathematical function with a low-standard deviation of values about the fit. Specifically, we show that using 1,000 measurements, and a heuristic method for choosing which links to measure, the RMS value of the errors in estimating link gains can be kept below 3 dB. As noted, the testbed environment we study is characterized by multipath and also by obstructions on many of the paths. To test our approach, we emulate the measurements of link gains by using WiSE, a ray-tracing tool developed by Bell Labs [8]. In addition to the perfect square grid on the ORBIT testbed, we also apply the proposed method to a similar lab with larger obstructions and an irregular node layout in a building with many obstructing walls. We find that, even for a difficult scenario with numerous obstructions, the partitioning method yields acceptably low-path gain estimation errors with a much-reduced number of measurements.

The rest of this paper is organized as follows. Models of both the environment and the node-to-node link gain (or pathloss) are given in Section 2. The new method for estimating link gains from limited measurements is described and exemplified in Section 3, and a method based on entropy is described for choosing the subset of transmitting nodes. In Section 4, two alternative, more complicated distributed network scenarios are postulated. For each, the entropy method for choosing transmitters and the new method for estimating link gains are applied, and numerical results are presented. Section 5 concludes the paper.

2. System Model

2.1. Classification of Link Gains. With the help of WiSE [8], we can obtain the set of all link gains for a specific environment as a function of its geometry. We have observed that in an indoor environment, the link gains deviate from the law of free-space propagation, due to the impacts of reflection, diffraction, and scattering. Furthermore, we have found that obstructed links, that is, those without a clear LOS path, usually undergo more severe attenuation than those with an LOS path, and the added attenuation caused by the obstructions is almost unrelated to the T-R separation distance [9].

Accordingly, the link between a given transmitter and receiver can be classified into one of several different categories according to the number of obstructing objects lying between them. A partition-based path loss analysis for in-home and residential areas at 5.85 GHz was conducted by Durgin et al. in [10]. In this paper, we generalize their framework to distributed wireless networks and propose to estimate both the path loss exponent and attenuation factors using selectively sampled measurements.

Consider the ORBIT testbed, for example, whose layout (top view) is shown in Figure 2. All the links are classified into three categories, namely, links having an LOS path, NLOS links traversing pillars only once, and NLOS links traversing pillars twice (there are no links traversing pillars three or more times in this particular grid). For convenience, in the following we will refer to the links in the three categories as types 0, 1, and 2, respectively.
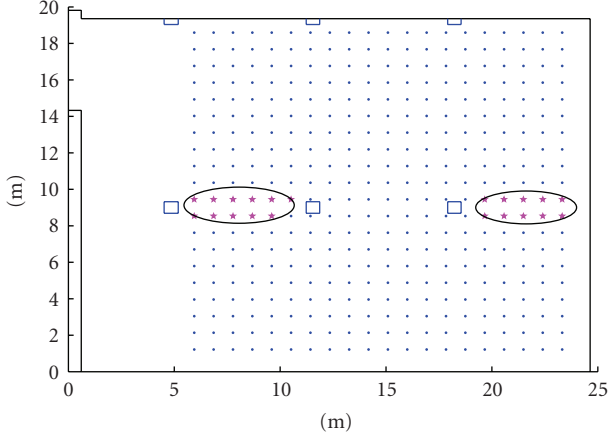
FIGURE 2: Top view of layout of 400-nodes ORBIT testbed. Both the vertical and horizontal dimensions are measured in meters (m). The three added rectangles in the middle represent obstructing pillars. The 21 transmitters highlighted with red stars and circled within ellipses serve transmit-receive links in all three categories. All other transmitters serve links in only the first and second categories.

More generally, let us assume that, in a given network of distributed wireless nodes, there are some paths between node pairs with as many as L different types of obstructions. Then, according to our approach, there will be $L + 1$ distinct categories (with one LOS category and L NLOS categories) for the pathloss formula, where pathloss is the negative dB value of link gain (received power divided by transmitted power). Assume that d_0 is a conveniently chosen reference distance, which is typically 1 meter in indoor environments; that $\epsilon(d_0)$ is the pathloss at d_0 for a single direct ray free-space pathloss; that α_l is the pathloss exponent for the lth category; that $PL_l(d)$ denotes the pathloss of type l at T-R separation distance d. A generalized expression for the LOS (type 0) and NLOS (type 1 to type L) pathloss estimate can be given by

$$PL_l(d) = \epsilon(d_0) + \Delta_l - 10\alpha_l\log_{10}\left(\frac{d}{d_0}\right), \quad 0 \le l \le L, \quad (1)$$

where $\epsilon(d_0) = 20\log_{10}(4\pi d_0/\lambda)$; λ is the wavelength; α_l is the pathloss exponent of type l links; Δ_l denotes an added increment resulting from multipath and for l obstructions.

3. Link Gain Matrix Estimation Based on Classified Links

3.1. MMSE Estimation for the Model Parameters. Assume $d_0 = 1$ m and that N_l measurements of path loss for links of type l are available, that is, $PL_l^0(d_i), i = 1, 2 \ldots, N_l$. Then the MMSE estimate for the pathloss exponent and attenuations can be obtained by solving

$$\left\{\hat{\alpha}_0, \ldots, \hat{\alpha}_L, \hat{\Delta}_0, \ldots, \hat{\Delta}_L\right\}$$

$$= \arg\min_{\underline{\alpha}, \underline{\Delta}}\left\{\sum_{l=0}^{L}\sum_{i=1}^{N_l}|\rho_l(\alpha_l, d_{l,i}) + \Delta_l|^2\right\}, \quad (2)$$

where $\underline{\alpha} := [\alpha_0 \cdots \alpha_L]$, $\underline{\Delta} := [\Delta_0 \cdots \Delta_L]$,

$$\rho_l(\alpha_l, d) = PL_l^0(d) - 10\alpha_l\log_{10}\left(\frac{d}{d_0}\right) + \varepsilon(d_0) \quad (3)$$

denotes the difference between the actual path loss (measured by equipment or emulated using ray tracing tools) and the estimate based on our model in (1).

For those links which are not measured, we can learn their T-R separations as well as their path type (i.e., value of l) through a simple geometric analysis. Then, by plugging the MMSE estimates into (1), the unknown link gains can be predicted.

3.2. A Heuristic Approach and Some Results. In order to achieve a good tradeoff between estimation accuracy and the complexity of measurement, an appropriate choice for the sampling set of link gains is important. Unfortunately, this is beyond the scope of classical sampling theory. Therefore, we need to resort to some heuristics.

To begin, let us consider the ORBIT testbed in Figure 2, which shows the 2-D top view of the 400-nodes. The three rectangles in the middle represent the obstructing pillars, and the uniformly-spaced dots denote the possible node locations. Through a simple geometrical calculation, we learned that to have a full diversity of links, that is, types 0, 1, and 2 all included, the transmitters have to be placed on one of the 21 locations (within the ellipses highlighted), while the remaining locations do not have type 2 links. Therefore, these 21 transmitter locations have more uncertainty than the remaining ones in terms of link types.

Our design is to measure a total of 1,000 link gains, and to do so by using transmitters at the 21 locations within the highlighted ellipses. Then we randomly choose 350, 600 and 50 samples from links of types 0, 1, and 2, respectively. The numbers of samples are chosen to be proportional to the total number of link gains in each category. This set of choices constitutes a trial. For each trial, we estimate the link gain model parameters via (2), and then substitute them into (1) to obtain the set of link gain estimates, say $\{PL_l^{\text{est}}\}$. For each transmitter-receiver pair on the grid, we employed the ray tracing result from WiSE as our benchmark set of type l link gain "measurements", say $\{PL_l\}$. The estimation error for a type l link is then given by

$$\varepsilon_l = PL_l^{\text{est}} - PL_l. \quad (4)$$

We repeat the above experiments for 100 trials.

For each type of link, we calculate the bias and standard deviations of ε, and plot them against the experimental trial index (1, 2,..., 100) in (a)-(b) of Figures 3, 4, and 5. (The estimation accuracy of type 2 NLOS links outperforms type 1 links in this example. This is because the number of sampled links versus the number of unmeasured links is greater for type 1 links with respect to our choice, that is, 50/(unmeasured number of type 2 links) > 600/(unmeasured number of type 1 links). Basically, the relative estimation accuracy for each category depend on how we allocate the ratio of samples for a given number of measurements. The general principle of selective sampling should guarantee
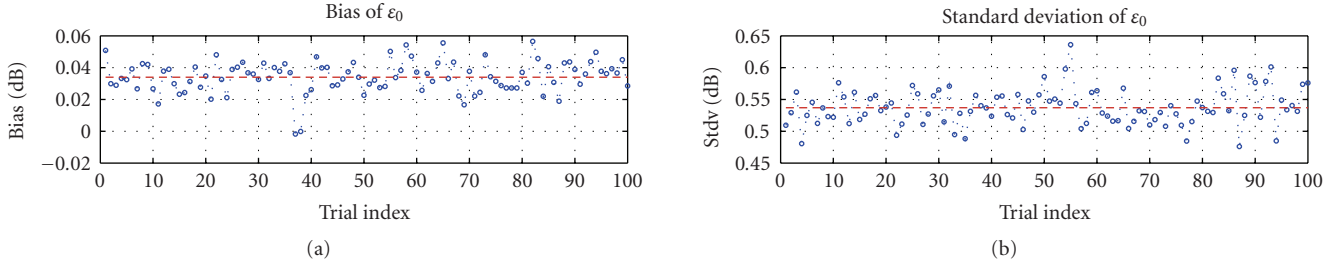
FIGURE 3: Statistics of estimation error for type 0 (LOS) links for 100 trial selection of sample measurements. The horizontal line is the average over the 100 trials. (a) Bias of ε_0, (b) Standard deviation of ε_0.
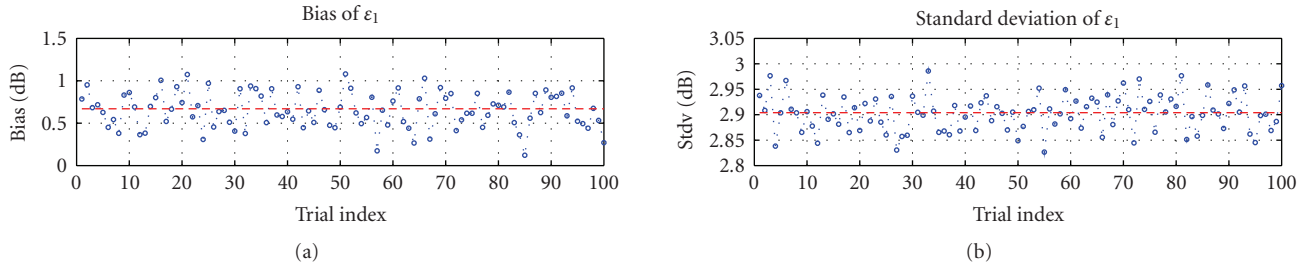

FIGURE 4: Statistics of estimation error for type 1 (NLOS) links for 100 trial selection of sample measurements. The horizontal line is the average over the 100 trials. (a) Bias of ε_1, (b) Standard deviation of ε_1.

the link gain estimation accuracy for every category.) The common value of α in these results was approximately 2.3. The solid lines in (a) and (b) denote the empirical bias and standard deviation for the estimation error ε, respectively; the dashed lines indicate the mean value over the 100 trials. We can conclude from these results that the random choice of $1,000$ link samples can provide sufficient estimation accuracy. (As a rule-of-thumb on testbed experimentation, calibration errors below 3 dB can be considered quite acceptable.). The method proposed in this paper outperforms spatial interpolation methods. In a separate computation not reported here, we have found that our proposed method, using 1/4 as many measurements, produces RMS estimation errors 3–4 dB lower than those using spatial interpolation.

3.3. Maximum Entropy Sampling. Despite the success of the heuristic strategy for the ORBIT testbed, for a more general setup a quantitative or semianalytic approach is desired. The first problem we need to solve is the selection of measurements. Given the size of samples, our objective is to select a most informative subset of link gains. As is traditional, we use entropy as our measure of information since it is a robust measure of the information available from a set of random variables [11]. To this end, let us assume that through site-specific analysis, the relative frequencies of type l link gains over the node ensemble of size $N(N-1)/2$ are known a priori, and are given by τ_l, $0 \le l \le L$. For links in each category, we characterize their "importance" or entropy by a constant [12]

$$\lambda_l = -\log_2 \tau_l. \tag{5}$$

As a consequence, the entropy of transmitter n can be quantized by the weighted sum of the $(N-1)$ TX-RX links propagating from it, that is,

$$\varpi(n) = \sum_{q=1}^{N} \sum_{l=0}^{L} \lambda_l \delta_{n,q}^l, \tag{6}$$

where

$$\delta_{n,q}^l = \begin{cases} 1, & \text{if link } (n,q) \text{ is of type } l, \\ 0, & \text{otherwise.} \end{cases} \tag{7}$$

Then the indices of transmitters, $\{n_l\}$, are rearranged according to their entropy, yielding

$$\varpi(n_1) \ge \varpi(n_2) \cdots \ge \varpi(n_N). \tag{8}$$

As a test for the proposed maximum-entropy sampling strategy, we calculated the empirical entropy for all the transmitter locations in Figure 2. It is not surprising that the 21 transmitter locations highlighted in Figure 2 stand out as the ones having the largest entropy.

In light of (8), we can identify the locations for the transmitter-receiver pairs whose link gains are going to be measured. Specifically, assume that χ is the total number of link gain measurements for a size N network, and that we will measure all the $N-1$ link gains between a transmitter, say n_l, and its $N-1$ receivers. We can choose $\kappa = \lfloor \chi/(N-1) \rfloor$ transmitter locations for sampling, which correspond to the first κ indices $\{n_l\}_{l=1}^{\kappa}$ in (8). Considering the reciprocity of link gains, κ is a lower bound for candidate transmitter locations. It is worth noting that spatial correlation is
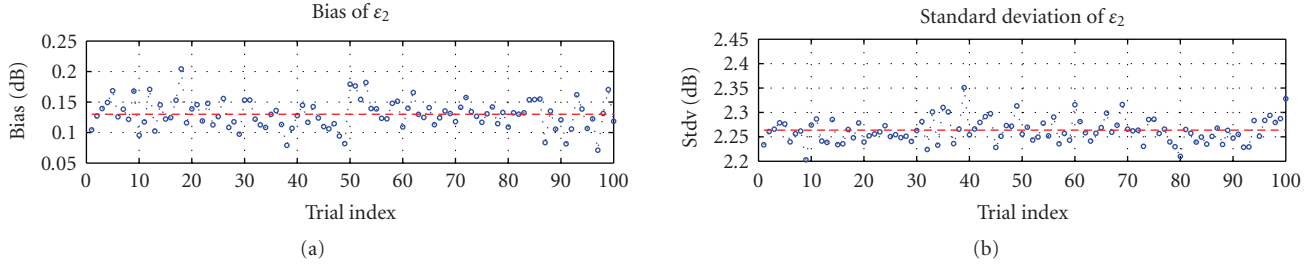
(a)

(b)

FIGURE 5: Statistics of estimation error for type 2 (NLOS) links for 100 trial selection of sample measurements. The horizontal line is the average over the 100 trials. (a) Bias of ε_2, (b) Standard deviation of ε_2.
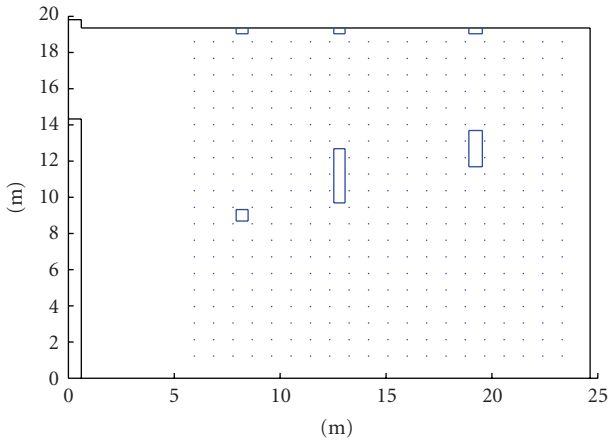

FIGURE 6: Layout of imaginary case with 400 nodes and three obstructers in the middle. Both the vertical and horizontal dimensions are measured in meters (m).
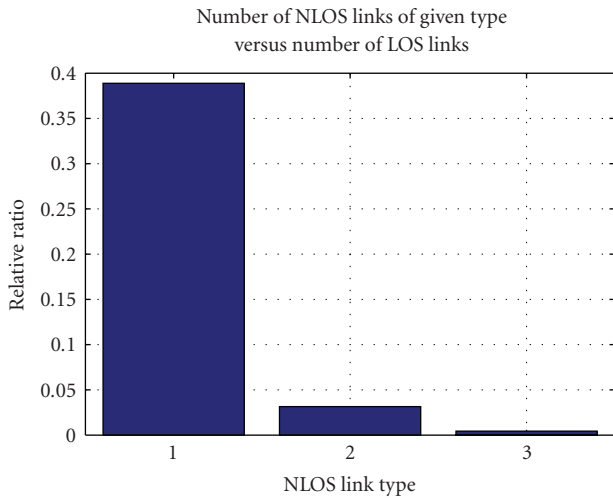

FIGURE 7: Relative size for the three types of NLOS links. For each type l ($l \geq 1$), the number of NLOS links is normalized by the number of LOS links (type 0).

not taken into account by (8). In other words, provided some of the nodes are close enough in space, the adjacent neighbors may exhibit similar entropy values because they are subject to very similar obstruction situations. To remove the redundancy incurred by spatial correlation, we can

employ a spatial mask over a sufficiently small area to "filter out" the node with representative entropy value and have it serve as the centroid of a clustered neighborhood.

4. Results for More Complex Scenarios

The results so far are for a fairly benign scenario: A 20×20 square grid in an open lab with three small obstructions. Here, we postulate two scenarios that are more difficult and evaluate the new method for each one, using the maximum-entropy strategy for selecting the links that are measured. The first scenario assumes an ORBIT-like testbed, except that the three obstructing pillars are irregularly placed and of various sizes. The second scenario assumes an irregular layout of 100 nodes distributed throughout an office building with 81 separation walls. Specifically, we consider the first floor of the Alcatel-Lucent building at Crawford Hill in Holmdel, New Jersey. This building has been the focus of numerous studies using the WiSE ray-tracing tool [13–15].

4.1. Modified Testbed Environment. As shown in Figure 6, the 400-nodes are still arranged into a 20 by 20 array, but the three pillars are reconfigured such that they are of different size and do not align with each other. In this experimental setup, all links are classified into four categories depending on the number of obstructions encountered. Specifically, the LOS links are denoted as type 0, whereas the NLOS links are grouped into type 1, type 2, and type 3, respectively. As shown in Figure 7, their relative frequencies (normalized by the number of LOS-type l links) are quite different, where the type 1 links significantly outnumber their type 2 and type 3 counterparts, resulting in their discrepancies of entropy.

In this exercise, we will specify $\chi \sim 8,000$ measurements, considerably more than the 1,000 measurements for the simpler, more regular ORBIT Lab. This means that there will be $\kappa = 20$ transmitting nodes, each sending signals to be measured by the other 399 nodes.

Figures 8(a)–8(c) enumerates the number of type 1, 2, and 3 links for each possible sampling location $n, 1 \leq n \leq 400$. Based on Figures 6 and 8, Figure 9 shows the entropy value for each possible transmitter location. It is obvious that our sampling of link gains can focus on a small set of transmitter locations only, namely, those with the largest entropies. The clustering around the spikes (local maxima) can be attributed to the spatial correlation among adjacent
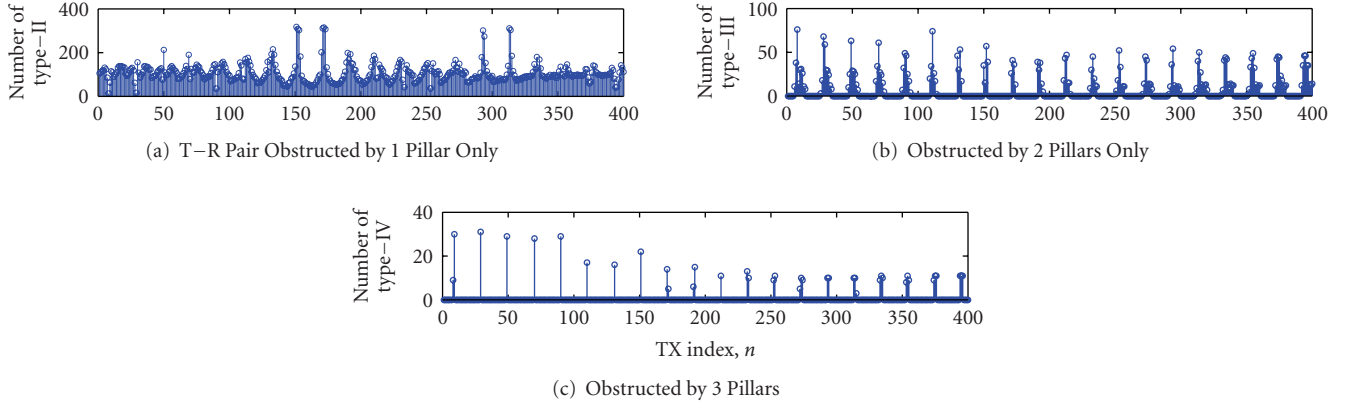
(a) T−R Pair Obstructed by 1 Pillar Only

(b) Obstructed by 2 Pillars Only

(c) Obstructed by 3 Pillars

FIGURE 8: Number of NLOS links in each category as a function of transmitter location. For convenience, the TX located on array coordinates (i, j), $1 \leq i$, $j \leq 20$ is indexed by $20 \times (i - 1) + j$.
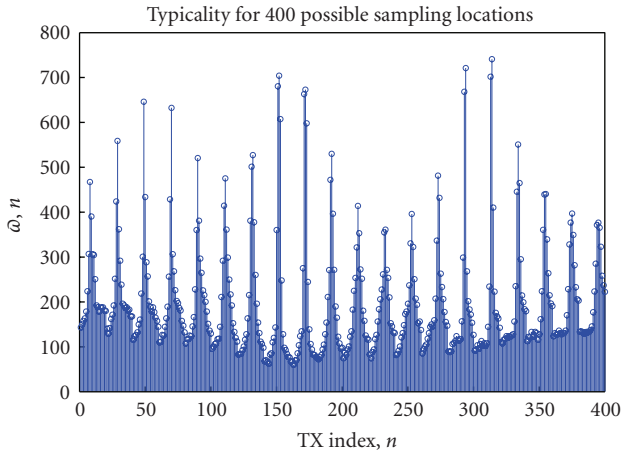

FIGURE 9: Entropy of each possible transmitter location.

transmitters. It can also be seen that there are 20 transmitter indices exhibiting local maximum values of typicality. We select these beacons for our experiment.

By sampling the link gains associated with the 20 transmitter locations ($\leq 20 \times 399$), we can obtain MMSE estimates for the LOS and NLOS pathloss exponents, attenuation factors, and then use them to predict the gains of all the unmeasured links. As a benchmark, we can collect the ensemble of pseudomeasurements given by ray tracing (using WiSE or other tools) and do the same estimation for modeling parameters as above. Figures 10(a), 10(b) and 10(c) compare the difference of these two approaches. The bar on the left corresponds to the full ensemble, which involves all the link gains obtained by ray tracing; while the bar on the right corresponds to the selected samples from the ensemble. Employing the full ensemble of link gains obtained by ray tracing, the estimation for the pathloss exponents and attenuation dB factors are given by $\alpha_0 = 2.0$, $\alpha_1 = 2.84$, $\alpha_2 = 2.93$, $\alpha_3 = 3.00$; and $\Delta_0 = 0.92$, $\Delta_1 = 4.98$, $\Delta_2 = 5.96$, $\Delta_3 = 6.13$, respectively. In contrast, by invoking the proposed "maximum entropy sampling" method, the estimation for the pathloss exponents and attenuation factors

are $\alpha_0 = 1.96$, $\alpha_1 = 2.86$, $\alpha_2 = 2.90$, $\alpha_3 = 2.98$; and $\Delta_0 = 1.15$, $\Delta_1 = 5.07$, $\Delta_2 = 5.93$, $\Delta_3 = 6.47$, respectively, which agree well with the previous derivations. We can see from these figures that, although the samples in the selected set are 10% of the ensemble size (200×399), the estimation accuracies for the pathloss parameters using the reduced set are within $\pm 8\%$ of the accuracies using the full set. Therefore, the efficacy of our selective sampling approach, which is based on the links' entropy, is verified.

4.2. Mesh Network in an Office Building. Figure 11 shows a top view of the first floor of the Crawford Hill building [13]. We assume that 100 wireless transceivers (nodes) are deployed in the offices and hallways with uniform randomness. Figure 12 is a scatter plot of pathloss versus distance for the nearly 5000 transmit-receive paths among the 100 nodes. The spread is large, but appropriate partitioning of the links can produce individual scatter plots of narrower spread.

Before proceeding, we note that there is a small number of weak links where the pathloss falls below 100 dB. As a rule-of-thumb, we can ignore any link in this category, since the pathloss is so large that the two nodes can be regarded as "disconnected". As a result, there are 4818 link gains to model, of which 590 are LOS (type 0) and 4228 are NLOS.

The 4228 NLOS links can be further partitioned into links with one or two intervening walls (type 1); links with three or four intervening walls (type 2); and links with more than four intervening walls (type 3). Figure 13 presents fitting parameters (α and Δ) and RMS fitting errors (δ) for two cases: in (a), all NLOS links are lumped into one category; and in (b), the NLOS links are partitioned, as above, into three categories. It is clear that the refined modeling corresponding to (b) provides a better fit to the scatter plots, since the average δ_l ($l = 0, \ldots, L$) is significantly reduced by increasing L. Little is gained in this case, however, by increasing L beyond 4.

Now assume a target of $\chi \sim 500$ link gain measurements, that is, about 10% of the total number of link gains. By applying the sampling methodology of Section 3.3, we can pick the five transmitter nodes with maximum entropy and

(a) Comparison of pathloss exponents

(b) Comparison of attenuation factors

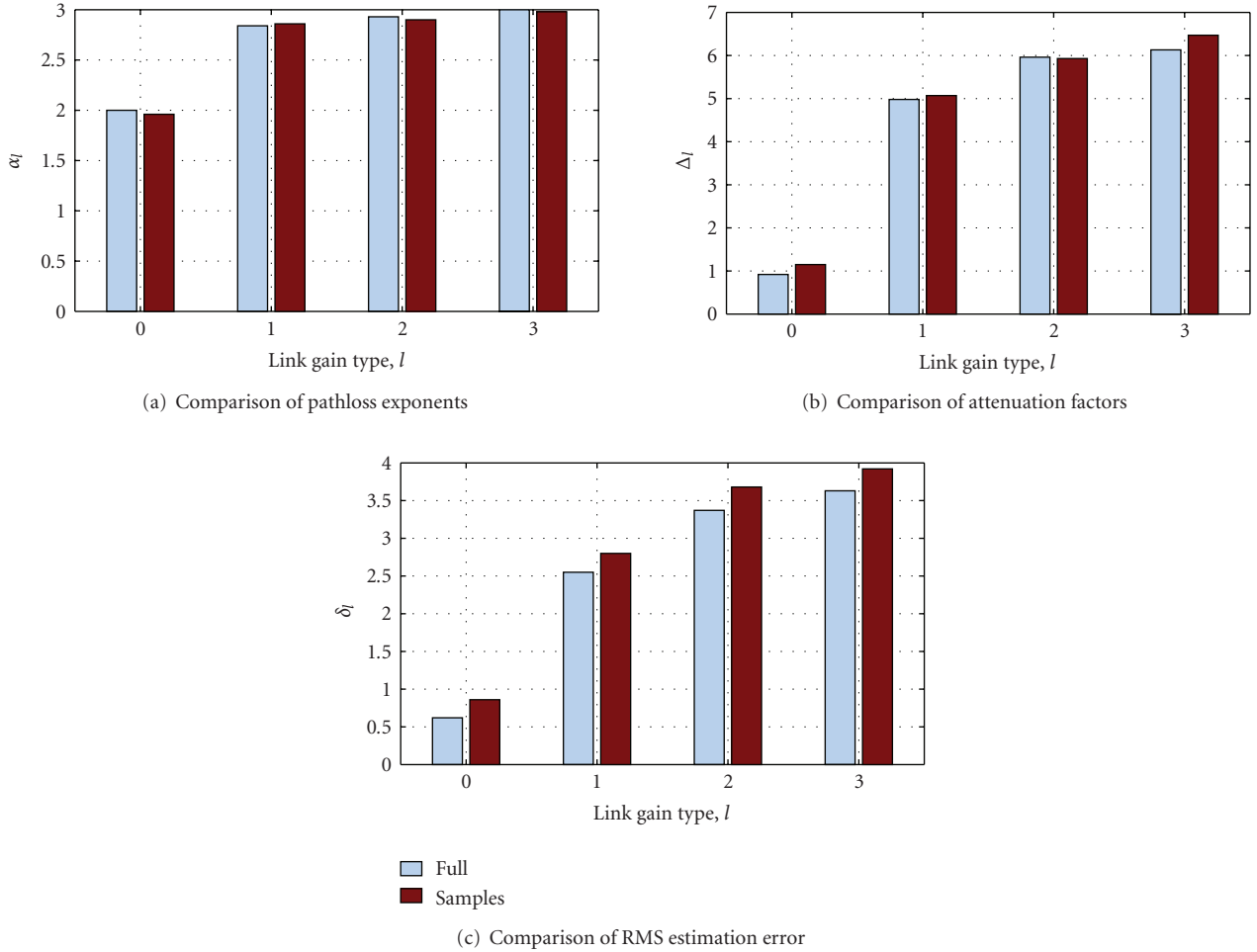Full
Samples

(c) Comparison of RMS estimation error

FIGURE 10: Comparison of Pathloss Model Parameters and RMS Estimation Error for the Experimental Setup in Figure 6.
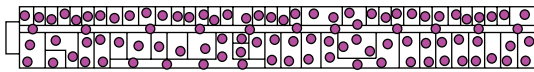

FIGURE 11: Top view of first floor of the Crawford Hill Building, with 100 nodes (filled circles) distributed with uniform randomness.

then measure their link gains (with respect to the rest of the network) to estimate the model parameters of (1). The outcome is shown in Figure 14, where the three bar graphs indicate the values of α, Δ, and RMS gain estimation error for each of the NLOS categories. The close agreements between the bars for the ensemble and those for the sample sets validate, again, the maximum-entropy approach for selecting transmitters. The RMS gain estimation errors are seen to be ~ 6 dB while, with all NLOS links lumped into one category, this error is close to 10 dB. This demonstrates the significant gain in accuracy by partitioning the NLOS links into several categories.

Most mesh network scenarios will probably have a complexity lying between the two extremes of the ORBIT Lab and the Crawford Hill example, above. In that case, the RMS
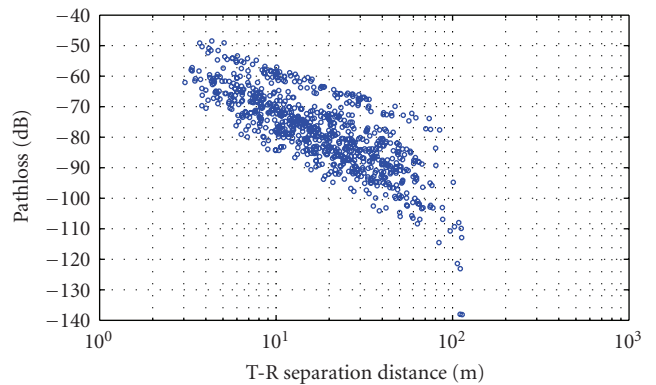

FIGURE 12: Scatter plot of pathloss versus log-distance for all node-to-node link gains inside the Crawford Hill Building (Figure 11). Most of the points near the top are for LOS paths.

gain estimation errors for most cases are likely to lie between 3 and 6 dB. The latter value might be reduced further, not by increasing L but by alternative, novel arrangements for choosing the links to be measured. This is a topic for further research.

Type−0 (LOS) $\{\alpha_0=1.92, \Delta_0=0\}$	Type−1 (NLOS) $\{\alpha_1=3.1, \Delta_1=8.36\}$
$\sigma_0=0.68$	$\sigma_1=9.54$

(a)

Type−0 (LOS) $\{\alpha_0=1.92, \Delta_0=0\}$	Type−1 (NLOS) $\{\alpha_1=2.56, \Delta_1=3.85\}$	Type−2 (NLOS) $\{\alpha_2=2.93, \Delta_2=5.26\}$	Type−3 (NLOS) $\{\alpha_3=3.18, \Delta_3=7.1\}$
$\sigma_0=0.68$	$\sigma_1=5.13$	$\sigma_2=5.77$	$\sigma_3=6.48$

(b)

FIGURE 13: Results for two ways of partitioning links in the Crawford Hill Building. (a) LOS links and all NLOS links. (b) LOS links and three categories of NLOS links, based on number of intervening walls. For each case, the results given are for the model parameters, α and Δ, and the fitting error, δ.

(a) Comparison of pathloss exponents

(b) Comparison of attenuation factors

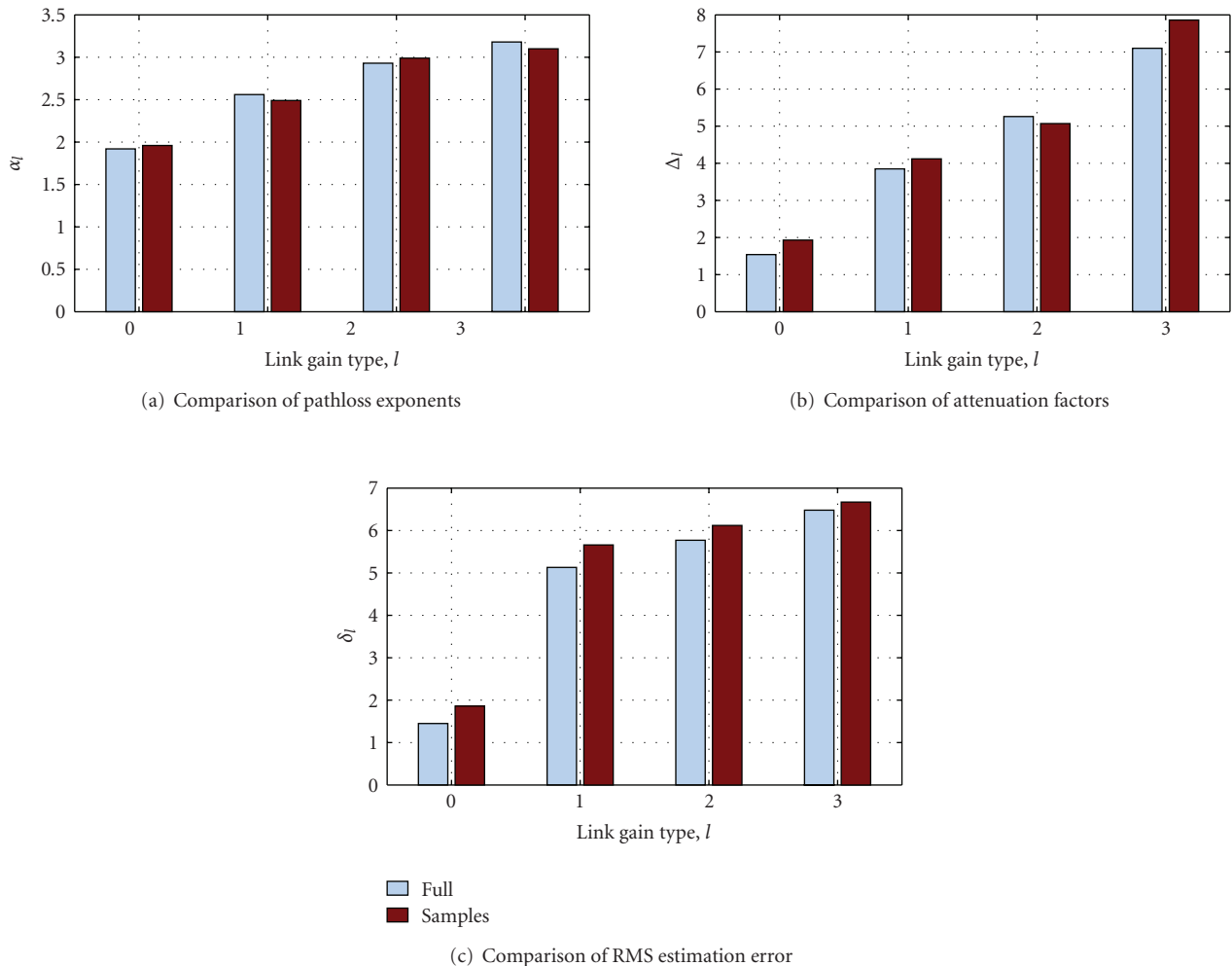
(c) Comparison of RMS estimation error

FIGURE 14: Model parameters and gain estimation errors for the Crawford Hill scenario in **Figure 11** with three NLOS categories. Results are shown for measurement of the full ensemble of link gains (left bars) and for measurement of a reduced set of 500 link gains (right bars). For the more conventional case where all NLOS links are lumped into one category, the RMS estimation error is close to 10 dB.

5. Conclusion

We have developed a link gain matrix estimation methodology for distributed nodes in wireless networks. In contrast to stochastic pathloss models with but one set of parameters, the proposed approach distinguishes among links with different numbers of path obstructions (or walls) and partitions them into separate models. We also developed a maximum-entropy method for selecting, in a structured way, the links to be measured. The results show that all gain matrix elements can be predicted with reasonable accuracy by measuring only a small fraction of all network links. Finally, the proposed method could be extended to outdoor networks, assuming the availability of site-specific data. This is due to the generality of the pathloss modeling, link partitioning, and transmitter selection approaches described here.

References

[1] I. F. Akyildiz, W. Su, Y. Sankarasubramaniam, and E. Cayirci, "A survey on sensor networks," *IEEE Communications Magazine*, vol. 40, no. 8, pp. 102–105, 2002.

[2] I. F. Akyildiz, X. Wang, and W. Wang, "Wireless mesh networks: a survey," *Computer Networks*, vol. 47, no. 4, pp. 445–487, 2005.

[3] J. Lei, R. Yates, L. Greenstein, and H. Liu, "Mapping link SNRs of real-world wireless networks onto an indoor testbed," *IEEE Transactions on Wireless Communications*, vol. 8, no. 1, pp. 157–165, 2009.

[4] J. Lei, R. Yates, L. Greenstein, and H. Liu, "Wireless link SNR mapping onto an indoor testbed," in *Procceddings of the 1st International Conference on Testbeds and Research Infrastructures for the Development of Networks and Communities (TRIDENTCOM '05)*, pp. 130–135, Trento, Italy, February 2005.

[5] J. Lei, R. Yates, L. Greenstein, and H. Liu, "Mapping link SNRs of wireless mesh networks onto an indoor testbed," in *Proceedings of the 2nd International Conference on Testbeds and Research Infrastructures for the Development of Networks and Communities (TRIDENTCOM '06)*, pp. 389–395, Barcelona, Spain, March 2006.

[6] V. Erceg, L. J. Greenstein, S. Y. Tjandra, et al., "Empirically based path loss model for wireless channels in suburban environments," *IEEE Journal on Selected Areas in Communications*, vol. 17, no. 7, pp. 1205–1211, 1999.

[7] X. Zhao, L. Razoumov, and L. J. Greenstein, "Path loss estimation algorithms and results for RF sensor networks," in *Proceedings of the 60th IEEE Vehicular Technology Conference (VTC '04)*, vol. 7, pp. 4593–4596, September 2004.

[8] S. J. Fortune, D. M. Gay, B. W. Kernighan, O. Landron, R. A. Valenzuela, and M. H. Wright, "WISE design of indoor wireless systems: practical computation and optimization," *IEEE Computational Science & Engineering*, vol. 2, no. 1, pp. 58–68, 1995.

[9] F. Aguado, F. Isasi, J. M. Hernando, A. Formella, and S. Pagel, "Interpolation techniques for ray-tracing models," *Microwave and Optical Technology Letters*, vol. 25, no. 5, pp. 343–346, 2000.

[10] G. D. Durgin, T. S. Rappaport, and H. Xu, "Partition-based path loss analysis for in-home and residential areas at 5.85 GHz," in *Proceedings of the IEEE Global Telecommunications Conference*, vol. 2, pp. 904–909, Sydney, Australia, 1998.

[11] V. Markl, P. J. Haas, M. Kutsch, N. Megiddo, U. Srivastava, and T. M. Tran, "Consistent selectivity estimation via maximum entropy," *The VLDB Journal*, vol. 16, no. 1, pp. 55–76, 2007.

[12] J. Lee, "Constrained maximum-entropy sampling," *Operations Research*, vol. 46, no. 5, pp. 655–664, 1998.

[13] R. A. Valenzuela, S. Fortune, and J. Ling, "Indoor propagation prediction accuracy and speed versus number of reflections in image-based 3-D ray-tracing," in *Proceedings of the 48th IEEE Vehicular Technology Conference (VTC '98)*, vol. 1, pp. 539–543, Ottawa, Canada, 1998.

[14] L. Xiao, L. Greenstein, N. Mandayam, and W. Trappe, "A physical-layer technique to enhance authentication for mobile terminals," in *Proceedings of IEEE International Conference on Communications (ICC '08)*, pp. 1520–1524, 2008.

[15] A. O. Kaya, L. Greenstein, D. Chizhik, R. Valenzuela, and N. Moayeri, "Emitter localization and visualization (ELVIS): a backward ray tracing algorithm for locating emitters," in *Proceedings og the 41st Annual Conference on Information Sciences and Systems (CISS '07)*, pp. 376–381, Baltimore, Md, USA, 2007.